Progress in Fractional Differentiation and Applications
An International Journal

http://dx.doi.org/10.18576/pfda/120204

Utilizing a Computational Fractional Method to Examine Permanganate's Oxidation of Sugars in Basic Aqueous Media

Muhammad Farman[1,2,3,*], *Aamir Shahzad*[1], *Abdul Sattar Ghaffari*[4], *Aseel Smerat*[5,6], *Muhammad Manan Akram* [7] *and Mohamed Hafez*[8,9]

[1] Mathematics Research Center, Department of Mathematics, Near East University, 99138 Nicosia, Turkey
[2] International Center for Interdisciplinary Research in Sciences, The University of Lahore, Lahore, Pakistan
[3] Research Center of Applied Mathematics, Khazar University, Baku, Azerbaijan
[4] Shifa Tameer-e-Millat University, Islamabad, Pakistan
[5] Faculty of Educational Sciences, Al-Ahliyya Amman University, Amman 19328, Jordan
[6] Department of Biosciences, Saveetha School of Engineering, Saveetha Institute of Medical and Technical Sciences, Chennai, 602105, India
[7] Washington university of Science and Technology, Washington, USA
[8] Faculty of Engineering and Quantity Surviving, INTI International University Colleges,71800, Nilai, Malaysia
[9] Faculty of Management, Shinawatra University, 12160, Pathum Thani, Thailand

Received: 8 Jan. 2026, Revised: 18 Feb. 2026, Accepted: 20 Mar. 2026
Published online: 1 Apr. 2026

Abstract: It is essential to comprehend the speeds and mechanisms of chemical reactions in chemistry, biology, and other disciplines. Sugars are one of the organic substrates that permanganate may oxidize, making it a crucial oxidant in both organic and inorganic redox reactions. By employing a literature reaction model to create a system of fractional order differential equations, this study investigates the significance of efficient oxidation procedures. It uses qualitative analysis of fractional order differential equations to explore possible permangantae oxidation pathways because there is not such research on these reactions. Using fixed point theorems, the model is examined and determined to be generalized Ulam-Hyers-Rassias stable. For solving fractional-order differential equations, especially in computer simulations including fractional operator effects, we employ the Laplace Adomian decomposition method (LADM), a reliable analytical and semi-analytical approach. Significant influence on the model's classes is demonstrated by graphs at various fractional derivative orders. The goal of the results is to enhance comprehension, process innovation and green product.

Keywords: Permanganate oxidation; Fractional-order mathematical model; Qualitative Analysis; Generalized Ulam-Hyers-Rassias Stability; Laplace Adomian Decomposition Method.

1 Introduction

Because of its efficacy and environmental friendliness, permanganate is a powerful and adaptable oxidizing agent in both organic and inorganic processes, and it is essential to green chemistry [1]. Because of its broad reactivity and capacity to oxidize organic substances via a variety of pathways, such as electron abstraction, hydrogen atom abstraction, hydride ion detachment, and oxygen exchange, relying on the substrate structure and the solution acidity, permanganate oxidation is an affordable and approachable environmental remediation technique [2]. Analytical approaches for determining oxidation levels in chemical and biological systems have been developed, with each employing particular indications or mechanisms [3,4]. Recent chemical oxidation techniques are being utilized to remove sulfonamide antibiotics from the aqueous phase, and Permanganate is commonly used to remove organic pollutants from wastewater. [5]. To improve the assessment of permanganate's applicability, the toxicity of breakdown products or intermediates in permanganate oxidation processes should be evaluated [6]. Because of its potent oxidizing ability and safe

* Corresponding author e-mail: farmanlink@gmail.com

characteristics, $KMnO_4$ is a ”green” oxidant that offers a long lasting and efficient remedy for chemical and environmental problems. It is frequently used because it is safer and easier to dose than ozonation and chlorination [7]. Because manganese can lead to aesthetic issues like staining and corrosion, the World Health Organization has recommended a maximum concentration limit of 0.4 mg/L for manganese in drinking water. In order to meet drinking water requirements, Mn(VII) is added to eliminate dissolved manganese and iron ions [8].

The importance of cyclic forms and enediols in a variety of mechanisms has been brought to light by the investigation of sugar oxidation kinetics in acidic and alkaline media (e.g., [9,10,11]). There are few investigations on the oxidation of sugar by metal ions or complexes in alkaline media; the oxidizing properties of potassium permanganate are mainly used, while the oxidation potential of $KMnO_4$ is seldom ever used [12]. Using differential and integral calculus, we mathematically simulate how the concentration of the reactants affects the order of chemical reactions. Designing oxidation techniques can be greatly aided by mathematical modeling and simulation [13,14,15]. By using mathematical methods to investigate chemical kinetics and enzyme reactions, several researchers have made important contributions to mathematical physiology and biochemistry [16,17,18]. In many disciplines, such as classical mechanics and contemporary control theory, stability analysis is crucial to comprehending and creating dynamic systems. It has a major impact on the design and analysis of linear and nonlinear systems, particularly higher order ones. In order to achieve exponential stability for complex-valued neural networks, research has concentrated on the problems of temporal delays and stochastic, impulsive effects [19,20].

Fractional calculus is gaining prominence due to its numerous applications in scientific and technical domains such as [21,22,23,24,25], notably in modeling complicated systems with memory and nonlocal dynamics. Position and momentum Shannon entropies function as metrics for uncertainty and spatial enclosing in their associated spaces in terms of the Fractional Schrödinger Equation (FSE), offering a broader description of quantum system attributes beyond the typical Heisenberg uncertainty concept [26,27,28]. Al-Basir et al. [29] developed an enzyme-kinetic mathematical model employing fractional order derivatives. Following the maximum principle, Euler-Lagrange optimality requirements were obtained for the fractional order control issue. Ali Akgül and Khoshnaw S. A. [30] discussed the fundamental principles of fractional differential equations and how they are applied to models of non-linear biological reactions. Singh et al. [31] investigated the dynamics of a triple collision and enzymatic reaction-diffusion system with a time-fractional Caputo derivative. Researchers [32] discussed a difficult nonlinear fractional model of an enzyme inhibitor reaction that takes into consideration reaction memory. CPC, a hybrid fractional operator that is more versatile than Caputo’s fractional derivative operator, was recently created by Baleanu et al. [33]. Naik et al. [34] used the chemistry and kinetics of enzymes to develop a fractional order mathematical model for chemical reactions. Using the constant proportional CF and ABC operators, this approach converts non-linear differential equations into fractional-order systems involving a two-step substrate-enzyme reversible process. The study [35] created a fractional order kinetic model to investigate the hydrogenolysis of glycerol, making sure that simulations matched the chemical structure involved in the reaction. The visualizations show that non-integer order has a major impact on solution curves performance and versatility. A Jacobi collocation method was proposed for the analysis of the fractional isothermal chemical model by Kumar et al. [36]. While comparing methods and examining mistakes, they worked through equations for various fractional orders of differentiation.

There is a lack of research on fractional order mathematical modeling for oxidation process of sugars through permanganate. This study resolves the model proposed in [37] using generalized proportional derivatives. The remaining sections of this manuscript are organized as follows: The model formulation and its conversion into fractional order using ideas from fractional calculus are covered in Section 2. The suggested model’s qualitative characteristics are examined in Section 3. We use the Laplace Adomian Decomposition Method in Section 4 to develop solutions to the proposed fractional order kinetic model. Sections 5 and 6 will go over numerical simulations, results and conclusions.

2 Model Formulation

A flexible oxidizing agent, permanganate is utilized to investigate the oxidation kinetics of different organic substrates. The authors propose a range of potential pathways that differ based on the reactive manganese species, reaction environment, and substrate. The organic substrates that permanganate can oxidize in this study are carbohydrates, or sugars. Here, we discuss a reaction mechanism [37] where the MnO_4^{2-} species undergoes a two-electron reduction as illustrated in Figure 1.

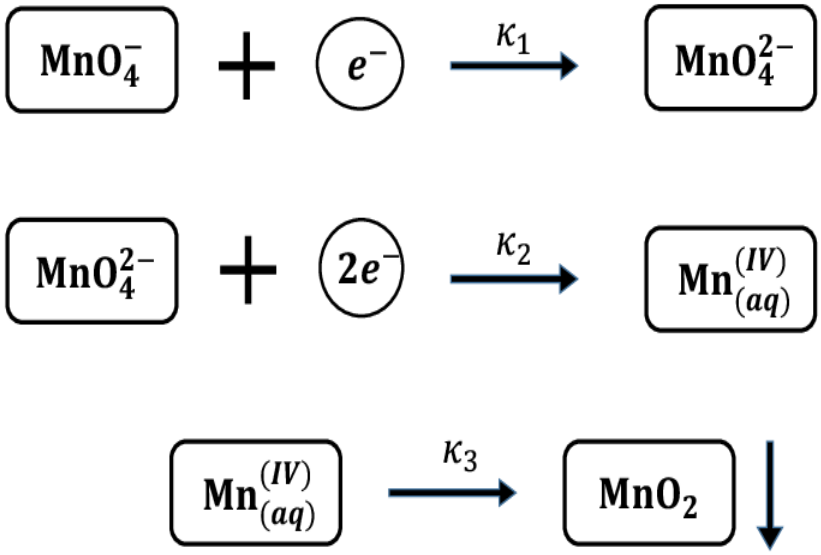

Fig. 1: The oxidation reaction mechanism

2.1 Kinetic Model

In the first process, permanganate $[Mn(VII)]$ is first reduced to manganate $[MnO_4^{2-}, Mn(VI)]$, and then $Mn^{(IV)}_{(aq)}$ is produced as a byproduct. In the last step, a soluble $Mn(IV)$ species is precipitated to create a colloidal suspension of MnO_2. The ODE's listed below would result from this mechanism:

$$\begin{aligned}
\frac{d\mathrm{M}_1}{dt} &= -\kappa_1 \mathrm{M}_1, \\
\frac{d\mathrm{M}_2}{dt} &= \kappa_1 \mathrm{M}_1 - \kappa_2 \mathrm{M}_2, \\
\frac{d\mathrm{M}_3}{dt} &= \kappa_2 \mathrm{M}_2 - \kappa_3 \mathrm{M}_3, \\
\frac{d\mathrm{M}_4}{dt} &= \kappa_3 \mathrm{M}_3,
\end{aligned} \tag{1}$$

where, $\mathrm{M}_1, \mathrm{M}_2, \mathrm{M}_3, \mathrm{M}_4$ represent MnO_4^-, MnO_4^{2-}, $Mn^{(IV)}_{(aq)}$, and MnO_2, respectively. The rate constants are given by k_i, $(i = 1,2,3)$. Rate constants (k_i) in this sugar oxidation model are variables that express how quickly or effectively each reaction occurs during the oxidation process.

2.2 Fractional-order Kinetic Model

Fractional calculus is essential for understanding complex system dynamics and controlling mathematical models. Fractional-order between 0 and 1 provides customizable time and frequency responses, enabling better performance. Following are certain important concepts of fractional calculus that will be used throughout the rest of this manuscript.

Definition 2.1. The Caputo derivative of a differentiable function $\Im(t)$ to order $\sigma \in (0,1)$ is defined [38] as

$$^{C}D_{t}^{\sigma}\Im(t) = \frac{1}{\Gamma(1-\sigma)}\int_{0}^{t}\Im'(\varphi)(t-\varphi)^{-\sigma}d\varphi. \tag{2}$$

Definition 2.2. With any integrable function $\Im(t)$ and $0 < \sigma < 1$, the Riemann-Liouville (RL) integral is defined [38] as

$$^{RL}D_{t}^{\sigma}\Im(t) = \frac{1}{\Gamma(\sigma)}\int_{0}^{t}(t-\varphi)^{\sigma-1}\Im(\varphi)d\varphi. \tag{3}$$

Definition 2.3. A novel type of fractional derivative, the constant-proportional-Caputo (CPC) fractional operator, has been identified by [33] as follows:

$$^{CPC}\mathrm{D}_{0,t}^{\sigma}\Im(t) = \frac{1}{\Gamma(1-\sigma)}\int_{0}^{t}\left[\gamma_1(\sigma)\Im(\varphi)+\gamma_0(\sigma)\Im'(\varphi)\right](t-\varphi)^{-\sigma}d\varphi \tag{4}$$

$$= \gamma_1(\sigma)\,^{RL}I_{0,t}^{1-\sigma}\Im(t)+\gamma_0(\sigma)\,^{C}D_{t}^{\sigma}\Im(t). \tag{5}$$

Definition 2.4. The CPC integral operator is defined [33] by

$$^{CPC}_{0}\mathrm{I}_{t}^{\sigma}\Im(t) = \frac{1}{\gamma_0(\sigma)}\int_{0}^{t}\exp\big(-\frac{\gamma_1(\sigma)}{\gamma_0(\sigma)}(t-\phi)\big)\,^{RL}_{0}\mathrm{D}_{\phi}^{1-\sigma}\Im(\phi)d\phi \tag{6}$$

Theorem 2.5. [33] The CPC operator's Laplace transform is:

$$\mathfrak{L}\big(^{CPC}_{0}\mathrm{D}_{t}^{\sigma}\Im(t)\big) = \big(\frac{\gamma_1(\sigma)}{S}+\gamma_0(\sigma)\big)s^{\sigma}\widehat{\Im}(S)-\gamma_0 s^{\sigma-1}\Im(0) \tag{7}$$

where $\Im(t)$ is a differentiable functions such that $\Im$ and $\Im'$ are locally L^1 for the Laplace transform on the positive reals $\widehat{\Im}$ exists.

Proof. Following from the Laplace transform, we have

$$\mathfrak{L}\big(^{RL}\mathrm{I}_{t}^{\sigma}\Im(t)\big) = s^{-\sigma}\widehat{\Im}(s), \qquad \mathfrak{L}\big(^{C}\mathrm{D}_{t}^{\sigma}\Im(t)\big) = s^{\sigma}\widehat{\Im}(s)-s^{\sigma-1}\Im(0) \tag{8}$$

for $0 < \sigma < 1$. Hence

$$\begin{aligned}\mathfrak{L}\big(^{CPC}_{0}\mathrm{D}_{t}^{\sigma}\Im(t)\big) &= \mathfrak{L}\big(\gamma_1(\sigma)^{RL}\mathrm{I}_{t}^{1-\sigma}\Im(t)+\gamma_0(\sigma)^{C}\mathrm{D}_{t}^{\sigma}\Im(t)\big)\\ &= \big(\gamma_1(\sigma)s^{\sigma-1}+\gamma_0 s^{\sigma}\big)\widehat{\Im}(s)-\gamma_0(\sigma)s^{\sigma-1}\Im(0),\end{aligned} \tag{9}$$

The previous system (1), by utilizing fractional-order derivative, is rewritten as

$$\begin{aligned}^{CPC}D_{0,t}^{\sigma}\big(\mathrm{M}_1(t)\big) &= -\kappa_1\mathrm{M}_1,\\ ^{CPC}D_{0,t}^{\sigma}\big(\mathrm{M}_2(t)\big) &= \kappa_1\mathrm{M}_1-\kappa_2\mathrm{M}_2,\\ ^{CPC}D_{0,t}^{\sigma}\big(\mathrm{M}_3(t)\big) &= \kappa_2\mathrm{M}_2-\kappa_3\mathrm{M}_3,\\ ^{CPC}D_{0,t}^{\sigma}\big(\mathrm{M}_4(t)\big) &= \kappa_3\mathrm{M}_3,\end{aligned} \tag{10}$$

where $^{CPC}D^{\sigma}$ represents the CPC derivative of order $0 < \sigma \leq 1$, and the initial conditions are

$$\mathrm{M}_1(0) = \mathrm{M}_{10} \geq 0,\ \ \mathrm{M}_2(0) = \mathrm{M}_{20} \geq 0,\ \ \mathrm{M}_3(0) = \mathrm{M}_{30} \geq 0,\ \ \mathrm{M}_4(0) = \mathrm{M}_{40} \geq 0.$$

In model (10), the range $\sigma \in (0,1]$ represents dynamics between a first-order rate process ($\sigma = 1$) and a constant rate process ($\sigma = 0$), representing memory effects, non-local associations, and atypical transmission in complex settings that are not described by integer-order models. Diffusion of sugar and oxygen frequently deviates from normal diffusion in complicated chemical environments, displaying anomalous diffusion. Fractional derivatives can be used to accurately describe this, taking long-range interactions and structural variability into consideration. Compared to traditional integer-order models that only take into account the current state, fractional-order models provide a more accurate representation of chemical systems, such as substance reactions in sugar oxidation, by taking into account non-local effects and the influence of the system's entire history. By enabling customizable time and frequency responses between 0 and 1, these

models enhance performance and provide improved control and comprehension of complicated system dynamics. Because the Caputo fractional derivative is compatible with classical beginning and boundary conditions, it is chosen over the RL derivative for practical physical issues. It is shown to be the best fractional operator for simulating memory and non-local interactions in various research domains. Its advantages are further increased by the CPC derivative, which makes complex dynamics modeling more flexible. By combining proportional and classical derivatives, the CPC derivative is a new operator that improves the model's ability to adapt to both current and past system conditions. It successfully addresses systems with non-constant memory effects or rate changes, including diffusion in non-homogeneous mediums, by defining a variety of processes. Interestingly, the CPC operator is a non-local, non-singular fractional operator that can be used to simulate processes such as sugar oxidation since it avoids singularity at the origin, captures memory effects, and may control the oxidation process by using a suitable fractional order ratio. Because of its unique characteristics and utilization, the CPC operator is a useful mathematical tool for modeling complicated pertinent issues (see, [39], [40], [41], [42]).

3 Qualitative analysis of the model

3.1 Boundedness and non-negativity of solutions

The proposed system's boundedness is characterized as follows:

$$^{CPC}D^{\sigma}_{0,t}\mathbf{S}(t) = {}^{CPC}D^{\sigma}_{0,t}\mathrm{M}_1(t) + {}^{CPC}D^{\sigma}_{0,t}\mathrm{M}_2(t) + {}^{CPC}D^{\sigma}_{0,t}\mathrm{M}_3(t) + {}^{CPC}D^{\sigma}_{0,t}\mathrm{M}_4(t). \tag{11}$$

Then,

$$^{CPC}D^{\sigma}_{0,t}\mathbf{S}(t) = 0, \quad 0 \leq \mathbf{S}(0) = J. \tag{12}$$

where $\mathbf{S}$ is the sum of system variables and J is any positive constant.
The following is the solution [33] to problem (12).

$$\mathbf{S}(t) \geq J\, e^{\left(-\frac{\lambda_1(\sigma)}{\lambda_0(\sigma)}\right)}. \tag{13}$$

This implies that $0 \leq \mathbf{S}(t)$ as $t \to \infty$.
$\Rightarrow$ The system (10)'s solutions are bounded.

Theorem 3.1. In $\mathbb{R}^4_+$, the proposed kinetic system (10)'s solution is unique and constrained under the initial conditions.
Proof. Under the initial conditions, it turns out that

$$^{CPC}D^{\sigma}_{0,t}[\mathrm{M}_1(t)]\big|_{\{\mathrm{M}_1=0\}} = 0, \tag{14}$$

$$^{CPC}D^{\sigma}_{0,t}[\mathrm{M}_2(t)]\big|_{\{\mathrm{M}_2=0\}} = \kappa_1\mathrm{M}_1 \geq 0, \tag{15}$$

$$^{CPC}D^{\sigma}_{0,t}[\mathrm{M}_3(t)]\big|_{\{\mathrm{M}_3=0\}} = \kappa_2\mathrm{M}_2 \geq 0, \tag{16}$$

$$^{CPC}D^{\sigma}_{0,t}[\mathrm{M}_4(t)]\big|_{\{\mathrm{M}_4=0\}} = \kappa_3\mathrm{M}_3 \geq 0, \tag{17}$$

Therefore, If

$$\{\mathrm{M}_1(0), \mathrm{M}_2(0), \mathrm{M}_3(0), \mathrm{M}_4(0)\} \in \mathbb{R}^4_+,$$

then there is no way for the solution to leave the hyperplane. Each hyperplane around the non-negative orthant has a vector field that points into the domain $\mathbb{R}^4_+$, which is a positively invariant set.

Remark 3.2. In order to match physical reality, non-negativity of solutions ensures that concentrations of chemical species be at least zero. The integrity and realism of simulations depend on this need. Boundedness guarantees that a system reaches a stable state, oscillates within a restricted range, or follows a predictable trajectory. An unbounded solution implies an impractical situation in which concentration could rise endlessly, which is not feasible in any actual chemical system.

3.2 Existence and Uniqueness Analysis

In order to prove the existence and uniqueness of solutions for system of differential equations in mathematical modeling, fixed point theorems are crucial mathematical tools. In real-world applications, a physical system behavior under specific initial conditions depends on the availability and uniqueness of solutions [43,44]. We established a rigorous proof for the existence and uniqueness of solutions to fractional differential equations in a chemical system using the Lipschitz condition and the Banach contraction principle, confirming that a related operator is a contraction mapping according to the Picard-Lindelöf theorem. Let's write the system (10) as follows:

$$\begin{cases} {}^{CPC}\mathrm{D}^{\sigma}_{0,t}\Pi(t) \;=\; \eta\big(t,\Pi(t)\big), \\ \qquad\quad \Pi(0) \;=\; \Pi_0 \geq 0, \quad 0<t<\mathbb{T}<\infty. \end{cases} \tag{18}$$

$\Pi(t)=(\mathrm{M}_1,\mathrm{M}_2,\mathrm{M}_3,\mathrm{M}_4)^{\mathrm{T}}$ represents the state variables, whereas η is a continuous function vector provided that:

$$\begin{pmatrix} \eta_1 \\ \eta_2 \\ \eta_3 \\ \eta_4 \end{pmatrix} = \begin{pmatrix} -\kappa_1\mathrm{M}_1, \\ \kappa_1\mathrm{M}_1-\kappa_2\mathrm{M}_2, \\ \kappa_2\mathrm{M}_2-\kappa_3\mathrm{M}_3, \\ \kappa_3\mathrm{M}_3, \end{pmatrix}, \tag{19}$$

with initial constraints Π_0. Additionally, η, a quadratic vector function, fulfils the Lipschitz condition, i.e., there exists $\mathfrak{E}\in\mathbb{R}$, such that

$$\Big\|\eta\big(t,\Pi_1(t)\big)-\eta\big(t,\Pi_2(t)\big)\Big\| \leq \mathfrak{E}\big\|\Pi_1(t)-\Pi_2(t)\big\|. \tag{20}$$

In a system of fractional differential equations, the Lipschitz condition is a crucial restriction on the function $\eta\big(t,\Pi(t)\big)$. In relation to $\Pi(t)$, this guarantees that the function $\eta\big(t,\Pi(t)\big)$ changes at a regulated rate. In proofs, it is used to show that the integral operator is a contraction mapping in an appropriate function space over a given period of time.

Theorem 3.2. If the following condition is true, the variable-order fractional suggested model (10) possesses a distinct solution.

$$\frac{\mathfrak{E}\mathscr{L}^{\sigma}_{\max}\mathscr{T}^{\sigma}_{\max}}{\gamma_0(\sigma)\Gamma(1-\sigma)}<1\,, \qquad t\in[0,\infty) \tag{21}$$

Proof. Utilizing (6) in (18), we find

$$\Pi(t)=\Pi(t_0)+\frac{1}{\gamma_0(\sigma)}\int_0^t \exp\big(-\frac{\gamma_1(\sigma)}{\gamma_0(\sigma)}(t-\varphi)\big){}^{RL}_{0}\mathrm{D}^{1-\sigma}_{\varphi}\eta(\varphi,\Pi(\varphi))d\varphi \tag{22}$$

Suppose that $\varpi=(0,\mathbb{T})$ and $\mathscr{B}:\mathrm{Z}(\varpi,\mathbb{R}^4_+)\to\mathrm{Z}(\varpi,\mathbb{R}^4_+)$. Then

$$\mathscr{B}\Pi(t)=\Pi(t_0)+\frac{1}{\gamma_0(\sigma)}\int_0^t \exp\big(-\frac{\gamma_1(\sigma)}{\gamma_0(\sigma)}(t-\varphi)\big){}^{RL}_{0}\mathrm{D}^{1-\sigma}_{\varphi}\eta(\varphi,\Pi(\varphi))d\varphi. \tag{23}$$

$$\Rightarrow \Pi(t)=\mathscr{B}\Pi(t). \tag{24}$$

Suppose that $\|*\|_{\varpi}$ is the supremum norm on K. Then

$$\big\|\Pi(t)\big\|_{\varpi}=\sup_{t\in\varpi}\|\Pi(t)\|, \qquad\qquad \Pi(t)\in\mathrm{Z}(\varpi,\mathbb{R}^4_+). \tag{25}$$

Therefore, with $\|*\|_{\varpi}$, $\mathrm{Z}(\varpi,\mathbb{R}^4_+)$ is a Banach space. The relation mentioned below is accurate.

$$\Big\|\int_0^t\rho(t,\varphi)d\varphi\Big\| \;\leq\; \big\|\rho(t,\varphi)\big\|_{\varpi}\,\big\|\Pi(s)\big\|_{\varpi}. \tag{26}$$

Where $\Pi(t)\in\mathrm{Z}(\varpi,\mathbb{R}^4_+)$, and $\rho(t,\varphi)\in\mathrm{Z}(\varpi^2,\mathbb{R}^4_+)$ which yields:

$$\big\|\rho(t,\varphi)\big\|_{\varpi}=\sup_{t,\varphi\in\varpi}\big|\rho(t,\varphi)\big\|. \tag{27}$$

We can write Equation (23) as:

$$\begin{cases} \left\|\mathscr{B}\Pi_1(t) & -\mathscr{B}\Pi_2(t)\right\|_{\varpi} \\ & \leq \left\| \frac{1}{\gamma_0(\sigma)} \int_0^t \exp\left(\frac{-\gamma_1(\sigma)}{\gamma_0(\sigma)}(t-\varphi)\right) \left[{}^{RL}_{0}\mathrm{D}_{\varphi}^{1-\sigma}\ \eta(\varphi,\Pi_1(\varphi))\right. \right. \\ & \qquad \left. \left. -{}^{RL}_{0}\mathrm{D}_{\varphi}^{1-\sigma}\ \eta(\varphi,\Pi_2(\varphi))\right] d\varphi \right\|_{\varpi} \\ & \leq \frac{\mathscr{X}_{\max}^{\sigma}}{\gamma_0(\sigma)\Gamma(1-\sigma)} \left\| \int_0^t (t-\varphi)^{\sigma-2} \left[\eta(\varphi,\Pi_1(\varphi)) - \eta(\varphi,\Pi_2(\varphi))\right] d\varphi \right\|_{\varpi} \\ & \leq \frac{\mathscr{X}_{\max}^{\sigma}\mathscr{T}_{\max}^{\sigma}}{\gamma_0(\sigma)\Gamma(1-\sigma)} \left\| \eta(\varphi,\Pi_1(\varphi)) - \eta(\varphi,\Pi_2(\varphi)) \right\|_{\varpi} \\ & \leq \frac{\mathfrak{C}\mathscr{X}_{\max}^{\sigma}\mathscr{T}_{\max}^{\sigma}}{\gamma_0(\sigma)\Gamma(1-\sigma)} \left\| \Pi_1(t) - \Pi_2(t) \right\|_{\varpi}. \end{cases} \tag{28}$$

Following this, we now have

$$\left\|\mathscr{B}\Pi_1(t) - \mathscr{B}\Pi_2(t)\right\|_{\varpi} \ \leq\ \mathbf{G}\left\|\Pi_1(t) - \Pi_2(t)\right\|_{\varpi}, \tag{29}$$

where $\mathbf{G} = \frac{\mathfrak{C}\mathscr{X}_{\max}^{\sigma}\mathscr{T}_{\max}^{\sigma}}{\gamma_0(\sigma)\Gamma(1-\sigma)}$.
The operator $\mathscr{B}$ is referred to be a contraction if $\mathbf{G} < 1$. System (10) then offers a unique solution.

3.3 Ulam-Hyers-Rassias (UHR) Stability

Here, we examine the Ulam-Hyers and generalized Ulam-Hyers-Rassias stability of (10).

Definition 3.1. Suppose that $\sigma \in (0,1)$ and let a continuous function $\eta : [0,\mathbb{T}] \to \mathbb{R}$. Afterwards, the proposed system (10) is said to be Ulam-Hyers stable if $\exists\ \mu, \chi > 0$ for every solution $\Pi \in \mathfrak{C}([0,\mathbb{T}],\mathbb{R})$ of (10)

$$\left|{}^{CPC}_{0}\mathrm{D}_t^{\sigma}\{\Pi(t)\} - \eta(t)\right| \leq \mu, \qquad \forall t \in [0,\mathbb{T}], \tag{30}$$

with a solution $\Theta \in \mathfrak{C}([0,\mathbb{T}],\mathbb{R})$ of (10) such that

$$|\Pi(t) - \Theta(t)| \leq \chi\mu, \qquad \forall t \in [0,\mathbb{T}]. \tag{31}$$

Definition 3.2. Assume that $\sigma \in (0,1)$, $\eta : [0,\mathbb{T}] \to \mathbb{R}$ and $\alpha : [0,\mathbb{T}] \to \mathbb{R}$ be continuous functions. Then, the system (10) is generalized Ulam-Hyers-Rassias stable if $\exists\ \zeta_{\eta,\alpha} > 0$ for every solution $\Pi \in \mathfrak{C}([0,\mathbb{T}],\mathbb{R})$ of (10) as

$$\left|{}^{CPC}_{0}\mathrm{D}_t^{\sigma}\Pi(t) - \eta(t)\right| \leq \alpha(t), \tag{32}$$

for all $t \in [0,\mathbb{T}]$ with a solution $\Theta \in \mathfrak{C}([0,\mathbb{T}],\mathbb{R})$ such that

$$|\Pi(t) - \Theta(t)| \leq \zeta_{\eta,\alpha}\ \alpha(t), \qquad \forall t \in [0,\mathbb{T}]. \tag{33}$$

Theorem 3.3. Let $\sigma \in (0,1)$, and a real function $\eta(t)$ on $[0,\mathbb{T}]$. If a function $\Pi : [0,\mathbb{T}] \to \mathbb{R}$ meets the following

$$\left|{}^{CPC}\mathrm{D}_{0,t}^{\sigma}\Pi(t) - \eta(t)\right| \leq \mu, \qquad \forall t \in [0,\mathbb{T}], \tag{34}$$

for each $t \in [0,\mathbb{T}]$ and $\mu > 0$ then system (10) has a solution $\Pi^{\bullet} : [0,\mathbb{T}] \to \mathbb{R}$ so that

$$|\Pi(t) - \Pi^{\bullet}(t)| \leq \left|\frac{1}{\gamma_0(\sigma)}\right| \left[\frac{\mathfrak{F}^{\sigma-2}}{\left|\Xi_1\Gamma(\sigma-2)\right|} + \left|\Xi_2\right|\ \mathfrak{F}\max\{1, e^{-\Xi_1 t}\}\right]\varsigma, \tag{35}$$

where $\Xi_1 = \frac{\gamma_0(\sigma)}{\gamma_1(\sigma)}$, and $\Xi_2 = \left(\frac{\gamma_1(\sigma)}{\gamma_0(\sigma)}\right)^{1-\sigma}$.

Proof. Suppose that

$$\mathrm{Z}(t) = {}^{CPC}\mathrm{D}_{0,t}^{\sigma}\Pi(t) - \eta(t), \qquad \forall t \in [0,\mathbb{T}] \tag{36}$$

Applying Laplace transform (7), we find

$$\begin{cases} \mathrm{Z}(s) = & \left(\frac{\gamma_1(\sigma)}{s} + \gamma_0(\sigma)\right) s^{\sigma}\widetilde{\Pi}(s) - \gamma_0(\sigma)s^{\sigma-1}\Pi(0) - \widetilde{\eta}(s) \\ & = \gamma_0(\sigma)\left(\Xi_1 + s\right)s^{\sigma-1}\widetilde{\Pi}(s) - \gamma_0(\sigma)s^{\sigma-1}\Pi(0) - \widetilde{\eta}(s). \end{cases} \tag{37}$$

We have

$$\begin{aligned}\widetilde{\Pi}(s) =& \frac{\Pi(0)}{\Xi_1+s}+\frac{1}{\gamma_0(\sigma)(\Xi_1+s)s^{\sigma-1}}\Big(\widetilde{\eta}(s)+\mathrm{Z}(s)\Big)\\ =& \frac{\Pi(0)}{\Xi_1+s}+\frac{1}{\gamma_0(\sigma)}\Big[\frac{1}{\Xi_1 s^{\sigma-1}}+\frac{\Xi_2}{\Xi_1+s}\Big]\Big(\widetilde{\eta}(s)+\mathrm{Z}(s)\Big).\end{aligned} \tag{38}$$

Let

$$\begin{aligned}\Pi^{\bullet}(t) =& \Pi^{\bullet}(0)e^{-\Xi_1 t}+\frac{1}{\gamma_0(\sigma)}\Big[\frac{1}{\Xi_1\Gamma(\sigma-2)}\int_0^t t^{\sigma-2}\ \eta(t-\varphi)d\varphi\\ &+\Xi_2\int_0^t e^{\Xi_1 t}\eta(t-\varphi)d\varphi\Big].\end{aligned} \tag{39}$$

Here, we use Laplace transform to (39) to get

$$\widetilde{\Pi}^{\bullet}(s)=\frac{\Pi^{\bullet}(0)}{\Xi_1+s}+\frac{1}{\gamma_0(\sigma)(\Xi_1+s)s^{\sigma-1}}\widetilde{\eta}(s). \tag{40}$$

As we know that

$$\mathfrak{L}\{{}_0^{CPC}\mathrm{D}_t^{\sigma}\Pi^{\bullet}(t)\}=\gamma_0(\sigma)(\Xi_1+s)s^{\sigma-1}\widetilde{\Pi}^{\bullet}(s)-\gamma_0(\sigma)s^{\sigma-1}\Pi^{\bullet}(0). \tag{41}$$

Putting (40) in (41), we have

$$\mathfrak{L}\{{}_0^{CPC}\mathrm{D}_t^{\sigma}\Pi^{\bullet}(t)\}=\widetilde{\eta}(s)=\mathfrak{L}\{\eta(t)\}. \tag{42}$$

$\Rightarrow$ Since $\mathfrak{L}$ is one-to-one, $\Pi^{\bullet}(t)$ is solution of (10).
From (38) and (40), we have

$$\widetilde{\Pi}(s)-\widetilde{\Pi}^{\bullet}(s)=\frac{1}{\gamma_0(\sigma)}\Big[\frac{1}{\Xi_1 s^{\sigma-1}}+\frac{\Xi_2}{\Xi_1+s}\Big]\mathrm{Z}(s). \tag{43}$$

Utilizing inverse Laplace transform, we find

$$\begin{cases}\Pi(t)-\Pi^{\bullet}(t) &= \mathfrak{L}^{-1}\{\widetilde{\Pi}(s)-\widetilde{\Pi}^{\bullet}(s)\}\\ &= \frac{1}{\gamma_0(\sigma)}\mathfrak{L}^{-1}\Big\{\Big[\frac{1}{\Xi_1 s^{\sigma-1}}+\frac{\Xi_2}{\Xi_1+s}\Big]\mathrm{Z}(s)\Big\}\\ &= \frac{1}{\gamma_0(\sigma)}\Big[\Big(\frac{t^{\sigma-2}}{\Xi_1\Gamma(\sigma-2)}\times\mathrm{Z}(t)\Big)+\Big(\Xi_2\ e^{-\Xi_1 t}\times\mathrm{Z}(t)\Big)\Big].\end{cases} \tag{44}$$

Hence,

$$\begin{cases}\big|\Pi(t)-\Pi^{\bullet}(t)\big| &= \frac{1}{|\gamma_0(\sigma)|}\Big[\frac{1}{|\Xi_1\Gamma(\sigma-2)|}\big|t^{\sigma-2}\times\mathrm{Z}(t)\big|+\big|\Xi_2\big|\ e^{-\Xi_1 t}\times\mathrm{Z}(t)\big|\Big]\\ &\le \frac{1}{|\gamma_0(\sigma)|}\Big[\frac{1}{|\Xi_1\Gamma(\sigma-2)|}\int_0^t\big|t^{\sigma-2}\big|\ \big|\mathrm{Z}(t-\varphi)\big|d\varphi\\ &+\big|\Xi_2\big|\ \int_0^t\big|e^{-\Xi_1 t}\big|\ \big|\mathrm{Z}(t-\varphi)\big|d\varphi\Big]\\ &\le \frac{1}{|\gamma_0(\sigma)|}\Big[\frac{1}{|\Xi_1\Gamma(\sigma-2)|}\varsigma\int_0^t\big|t^{\sigma-2}\big|d\varphi+\big|\Xi_2\big|\ \varsigma\int_0^t\big|e^{-\Xi_1 t}\big|d\varphi\Big]\\ &\le \frac{1}{|\gamma_0(\sigma)|}\Big[\frac{\mathfrak{F}^{\sigma-2}}{|\Xi_1\Gamma(\sigma-2)|}+\big|\Xi_2\big|\ \mathfrak{F}\max\big\{1,e^{-\Xi_1 t}\big\}\Big]\varsigma.\end{cases} \tag{45}$$

The system (10) is therefore Ulam-Hyers stable with the constant

$$\wp=\frac{1}{|\gamma_0(\sigma)|}\Big[\frac{\mathfrak{F}^{\sigma-2}}{|\Xi_1\Gamma(\sigma-2)|}+\big|\Xi_2\big|\ \mathfrak{F}\max\big\{1,e^{-\Xi_1 t}\big\}\Big]. \tag{46}$$

Theorem 3.4. Let $\sigma\in(0,1)$ and a real function $\eta(t)$ on $[0,\mathbb{T}]$. If any function $\Pi:[0,\mathbb{T}]\to\mathbb{R}$ meets the following

$$\big|{}_0^{CPC}\mathrm{D}_t^{\sigma}\Pi(t)-\eta(t)\big|\le\alpha(t),\qquad \forall t\in[0,\mathbb{T}], \tag{47}$$

then we have

$$\mathrm{Z}(t)\le\alpha(t),\qquad \forall t\in[0,\mathbb{T}],\quad \mu>0. \tag{48}$$

Proof. There is a solution $\Pi^{\bullet}:[0,\mathbb{T}]\to\mathbb{R}$ of (10) that is consistent with Theorem (34):

$$\Pi(t)-\Pi^{\bullet}(t)=\frac{1}{\gamma_0(\sigma)}\Big[\Big(\frac{t^{\sigma-2}}{\Xi_1\Gamma(\sigma-2)}\times \mathrm{Z}(t)\Big)+\Big(\Xi_2\, e^{-\Xi_1 t}\times \mathrm{Z}(t)\Big)\Big]. \tag{49}$$

and

$$\begin{aligned}
\big|\Pi(t)-\Pi^{\bullet}(t)\big| &= \frac{1}{|\gamma_0(\sigma)|}\Big[\frac{1}{\big|\Xi_1\Gamma(\sigma-2)\big|}\big|t^{\sigma-2}\times \mathrm{Z}(t)\big|+\big|\Xi_2\big|\,\big|e^{-\Xi_1 t}\times \mathrm{Z}(t)\big|\Big]\\
&\le \frac{1}{|\gamma_0(\sigma)|}\Big[\frac{1}{\big|\Xi_1\Gamma(\sigma-2)\big|}\big|t^{\sigma-2}\big|\int_0^t \big|\mathrm{Z}(t-\varphi)\big|d\varphi\\
&\qquad +\big|\Xi_2\big|\,\mathfrak{F}\max\big\{1,e^{-\Xi_1 t}\big\}\int_0^t\big|\mathrm{Z}(t-\varphi)\big|d\varphi\Big]\\
&\le \frac{1}{|\gamma_0(\sigma)|}\Big[\frac{\mathfrak{F}^{\sigma-2}}{\big|\Xi_1\Gamma(\sigma-2)\big|}\big|\mathrm{Z}(t)\big|+\big|\Xi_2\big|\,\mathfrak{F}\max\big\{1,e^{-\Xi_1 t}\big\}\big|\mathrm{Z}(t)\big|\Big]\\
&\le \frac{1}{|\gamma_0(\sigma)|}\Big[\frac{\mathfrak{F}^{\sigma-2}}{\big|\Xi_1\Gamma(\sigma-2)\big|}+\big|\Xi_2\big|\,\mathfrak{F}\max\big\{1,e^{-\Xi_1 t}\big\}\Big]\alpha(t),
\end{aligned} \tag{50}$$

under the condition $\int_0^t\big|\mathrm{Z}(t)\big|d\varphi\le \mathrm{Z}(t)$, for any $t\in[0,\mathbb{T}]$.
In view of α on $[0,\mathbb{T}]$, the system (10) is generalized Ulam-Hyers-Rassias stable.

4 Numerical Solution

By utilizing Theorem [33] and implementing the Laplace transform to both ends of equations (10), the result is

$$\begin{cases}
\mathfrak{L}\{\mathrm{M}_1(t)\}=\frac{\mathrm{M}_1(0)}{s+\frac{\gamma_1(\sigma)}{\gamma_0(\sigma)}}+\frac{1}{\gamma_0(\sigma)}\sum_{j=0}^{\infty}\big(\frac{-\gamma_1(\sigma)}{\gamma_0(\sigma)}\big)^{j+1}s^{-\sigma-j}\big(-\kappa_1\mathfrak{L}\{\mathrm{M}_1\}\big),\\
\mathfrak{L}\{\mathrm{M}_2(t)\}=\frac{\mathrm{M}_2(0)}{s+\frac{\gamma_1(\sigma)}{\gamma_0(\sigma)}}+\frac{1}{\gamma_0(\sigma)}\sum_{j=0}^{\infty}\big(\frac{-\gamma_1(\sigma)}{\gamma_0(\sigma)}\big)^{j+1}s^{-\sigma-j}\big(\kappa_1\mathfrak{L}\{\mathrm{M}_1\}-\kappa_2\mathfrak{L}\{\mathrm{M}_2\}\big),\\
\mathfrak{L}\{\mathrm{M}_3(t)\}=\frac{\mathrm{M}_3(0)}{s+\frac{\gamma_1(\sigma)}{\gamma_0(\sigma)}}+\frac{1}{\gamma_0(\sigma)}\sum_{j=0}^{\infty}\big(\frac{-\gamma_1(\sigma)}{\gamma_0(\sigma)}\big)^{j+1}s^{-\sigma-j}\big(\kappa_2\mathfrak{L}\{\mathrm{M}_2\}-\kappa_3\mathfrak{L}\{\mathrm{M}_3\}\big),\\
\mathfrak{L}\{\mathrm{M}_4(t)\}=\frac{\mathrm{M}_4(0)}{s+\frac{\gamma_1(\sigma)}{\gamma_0(\sigma)}}+\frac{1}{\gamma_0(\sigma)}\sum_{j=0}^{\infty}\big(\frac{-\gamma_1(\sigma)}{\gamma_0(\sigma)}\big)^{j+1}s^{-\sigma-j}\big(\kappa_3\mathfrak{L}\{\mathrm{M}_3\}\big).
\end{cases} \tag{51}$$

The scheme provides outcomes as an infinite series:

$$\mathrm{M}_1(t)=\sum_{k=0}^{\infty}\mathrm{M}_{1k},\quad \mathrm{M}_2(t)=\sum_{k=0}^{\infty}\mathrm{M}_{2k},\quad \mathrm{M}_3(t)=\sum_{k=0}^{\infty}\mathrm{M}_{3k},\quad \mathrm{M}_4(t)=\sum_{k=0}^{\infty}\mathrm{M}_{4k}. \tag{52}$$

After some calculations, we get finally the following iterative solutions

$$\begin{cases}
\mathrm{M}_{1k+1}(t) &= \mathrm{M}_1(0)\exp\Big(\frac{-\gamma_1(\sigma)}{\gamma_0(\sigma)}t\Big)+\frac{1}{\gamma_0(\sigma)}\sum_{j=0}^{\infty}\Big(\frac{-\gamma_1(\sigma)}{\gamma_0(\sigma)}\Big)^{j+1}\frac{t^{\sigma+j-1}}{\Gamma(\sigma+j)}\\
&\quad\times\mathfrak{L}^{-1}\Big\{-\kappa_1\mathfrak{L}\{\mathrm{M}_{1k}\}\Big\},\\
\mathrm{M}_{2k+1}(t) &= \mathrm{M}_2(0)\exp\Big(\frac{-\gamma_1(\sigma)}{\gamma_0(\sigma)}t\Big)+\frac{1}{\gamma_0(\sigma)}\sum_{j=0}^{\infty}\Big(\frac{-\gamma_1(\sigma)}{\gamma_0(\sigma)}\Big)^{j+1}\frac{t^{\sigma+j-1}}{\Gamma(\sigma+j-1)}\\
&\quad\times\mathfrak{L}^{-1}\Big\{\kappa_1\mathfrak{L}\{\mathrm{M}_1\}-\kappa_2\mathfrak{L}\{\mathrm{M}_2\}\Big\},\\
\mathrm{M}_{3k+1}(t) &= \mathrm{M}_3(0)\exp\Big(\frac{-\gamma_1(\sigma)}{\gamma_0(\sigma)}t\Big)+\frac{1}{\gamma_0(\sigma)}\sum_{j=0}^{\infty}\Big(\frac{-\gamma_1(\sigma)}{\gamma_0(\sigma)}\Big)^{j+1}\frac{t^{\sigma+j-1}}{\Gamma(\sigma+j-1)}\\
&\quad\times\mathfrak{L}^{-1}\Big\{\kappa_2\mathfrak{L}\{\mathrm{M}_2\}-\kappa_3\mathfrak{L}\{\mathrm{M}_3\}\Big\},\\
\mathrm{M}_{4k+1}(t) &= \mathrm{M}_4(0)\exp\Big(\frac{-\gamma_1(\sigma)}{\gamma_0(\sigma)}t\Big)+\frac{1}{\gamma_0(\sigma)}\sum_{j=0}^{\infty}\Big(\frac{-\gamma_1(\sigma)}{\gamma_0(\sigma)}\Big)^{j+1}\frac{t^{\sigma+j-1}}{\Gamma(\sigma+j-1)}\\
&\quad\times\mathfrak{L}^{-1}\Big\{\kappa_3\mathfrak{L}\{\mathrm{M}_3\}\Big\}.
\end{cases} \tag{53}$$

5 Result and Discussion

The Laplace Adomian decomposition method and the parametric values from [37] have been used to perform numerical simulations of the model. Figures 2-13 show the simulations of the proposed fractional order kinetic model utilizing different fractional order values $\sigma = 1.0, 0.95, 0.90, 0.85$. The kinetic variables of the permanganate oxidation of sugars in a basic water-soluble medium at room temperature are listed in detail in Table (1) from a prior work [37].

Fructose date simulations of the model compartments for different fractional orders under the CPC operator are displayed in Fig. 2,3,4,5. This indicates that for low fractional orders, the first reduction of permanganate to manganate proceeds more quickly. At lower fractional orders, MnO_4^- falls and quickly transforms to MnO_4^{2-}. High fractional orders yield MnO_4^{2-}, which quickly transforms into $Mn_{(aq)}^{(IV)}$. Finally, $Mn_{(aq)}^{(IV)}$ changes into MnO_2 faster and with smaller fractional order. Convergence of the fructose data set to a physically meaningful respond requires the initial parameters to be chosen quite carefully. The size and absorption spectra of MnO_2 nanoparticles vary over time due to the unregulated nature of their synthesis in experimental settings.

Using glucose data, the model compartments are simulated for different fractional orders under the CPC operator in Fig. Fig. 6,7,8,9. At lower fractional orders, the concentration of MnO_4^- falls and rapidly converts to MnO_4^{2-}. At low fractional orders, MnO_4^{2-} is quickly generated and rapidly converts into $Mn_{(aq)}^{(IV)}$. Finally, with smaller fractional order, $Mn_{(aq)}^{(IV)}$ converts faster into MnO_2.

For different fractional orders, the model compartments with sucrose date are simulated under the CPC operator in Fig. 10,11,12,13. At smaller fractional orders, the concentration of MnO_4^- decreases and quickly turns into MnO_4^{2-}. At low fractional orders, MnO_4^{2-} quickly forms and transforms into $Mn_{(aq)}^{(IV)}$. Finally, with less fractional order, $Mn_{(aq)}^{(IV)}$ change quicker to MnO_2. Compared to glucose and fructose, MnO_4^- transforms into MnO_2 much faster. Since glucose and fructose are joined by an anomeric carbon to form sucrose, it is a non-reducing dimer. Its initial electron transfer rates are slower than those of glucose and fructose. This slows down the reaction by making sucrose harder to oxidize.

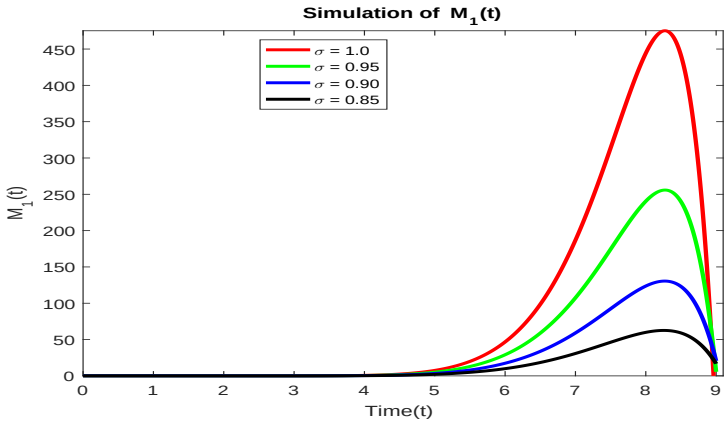

Fig. 2: Simulation of MnO_4^- using fructose data at CPC operator

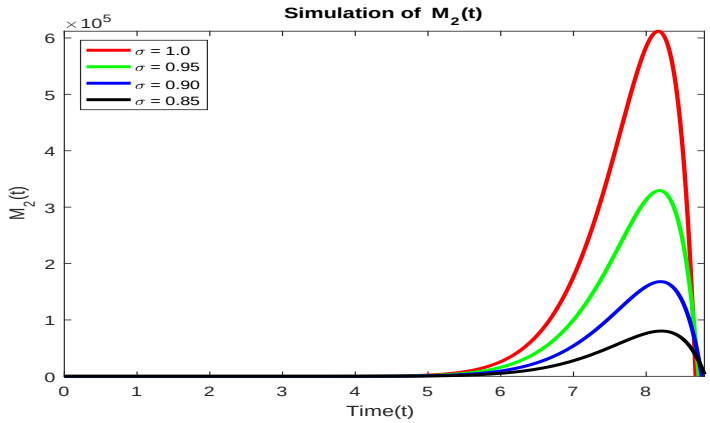

Fig. 3: Simulation of MnO_4^{2-} using fructose data at CPC operator

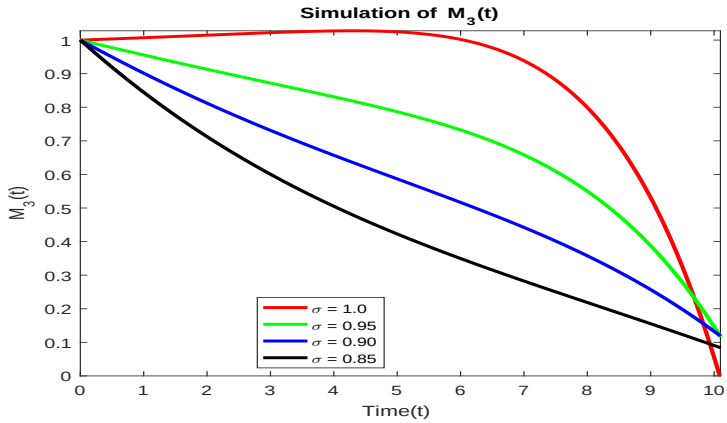

Fig. 4: Simulation of $Mn_{(aq)}^{(IV)}$ using fructose data at CPC operator

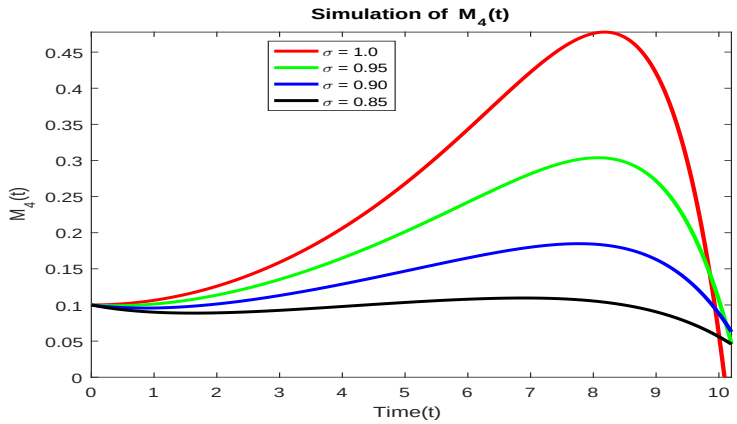

Fig. 5: Simulation of MnO_2 using fructose data at CPC and Caputo operator

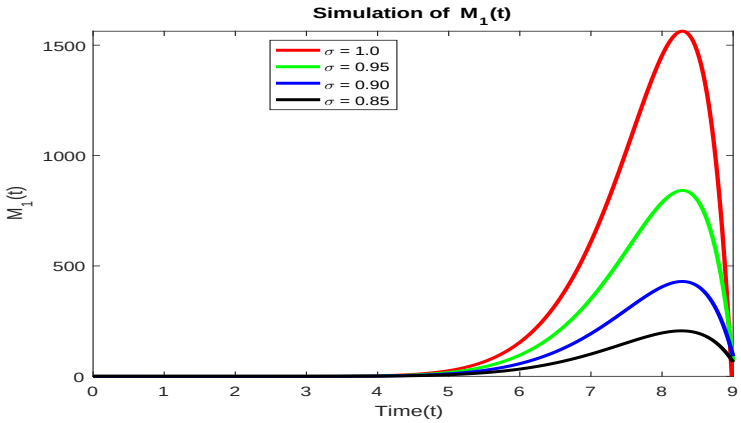

Fig. 6: Simulation of MnO_4^- using glucose data at CPC operator

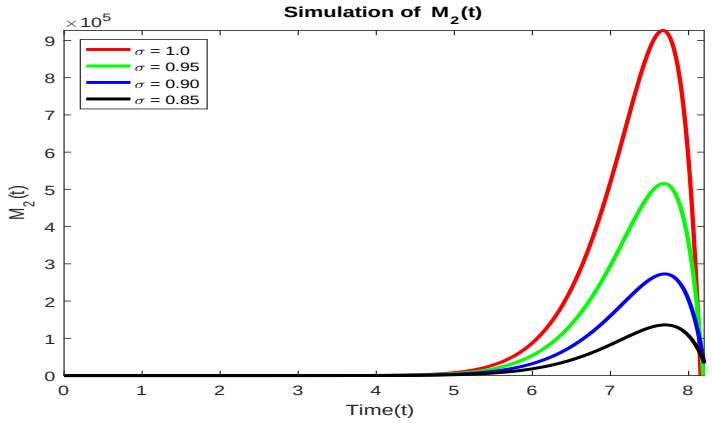

Fig. 7: Simulation of MnO_4^{2-} using glucose data at CPC operator

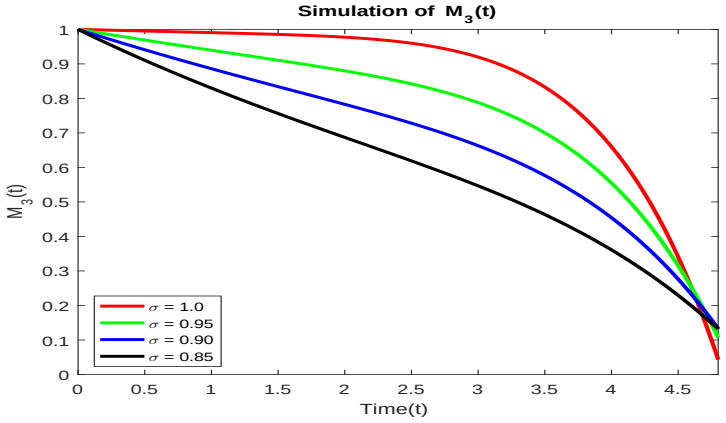

Fig. 8: Simulation of $Mn_{(aq)}^{(IV)}$ using glucose data at CPC operator

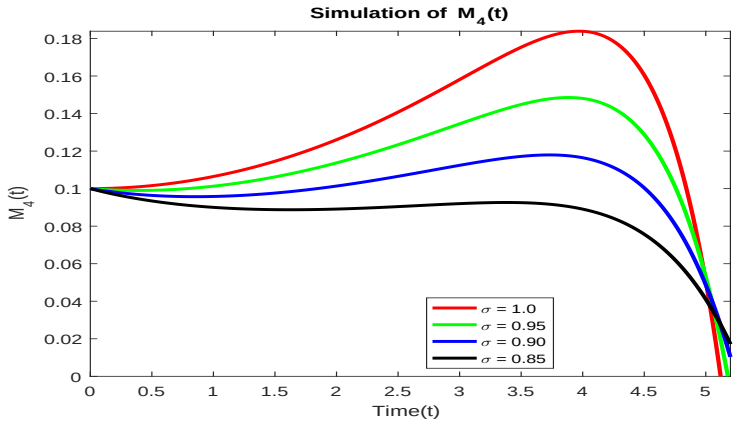

Fig. 9: Simulation of MnO_2 using glucose data at CPC and Caputo operator

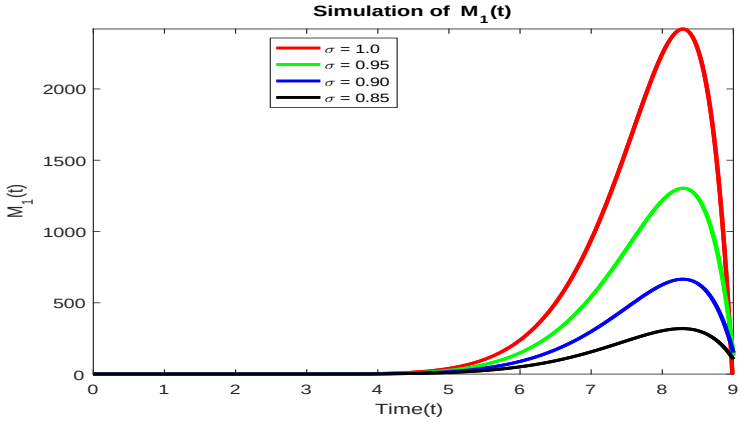

Fig. 10: Simulation of MnO_4^- using sucrose data at CPC operator

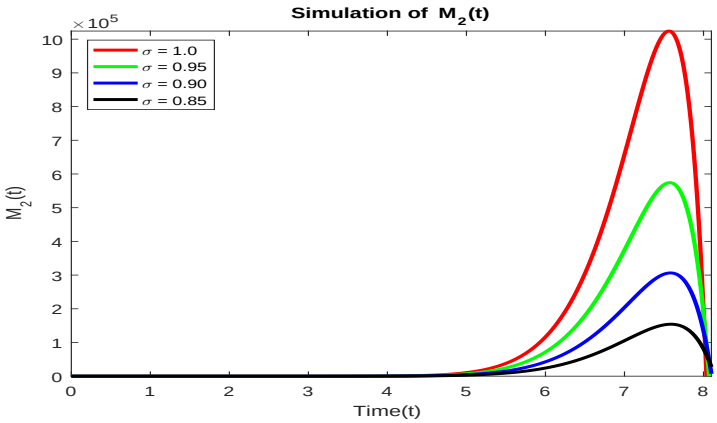

Fig. 11: Simulation of MnO_4^{2-} using sucrose data at CPC operator

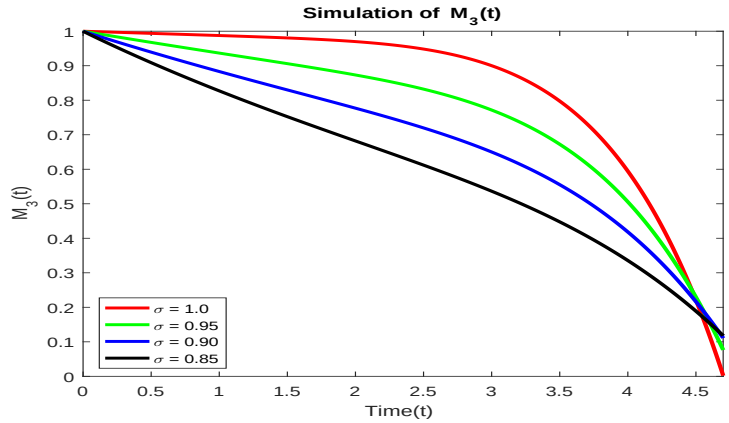

Fig. 12: Simulation of $Mn^{(IV)}_{(aq)}$ using sucrose data at CPC operator

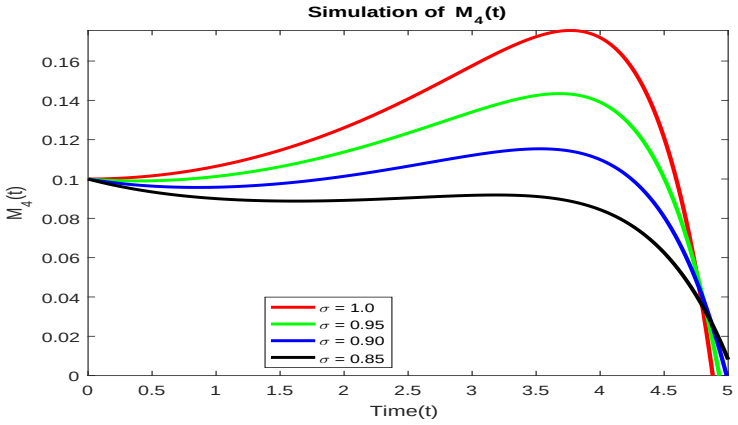

Fig. 13: Simulation of MnO_2 using sucrose data at CPC and Caputo operator

At lower fractional orders, the conversion process occurs more rapidly, necessitating an understanding of kinetic systems dynamics. It is essential to comprehend the previous chemical processes to assess the formation range of MnO_2. Fractional order models yield superior predictions for long-range interactions among permanganate species, with accelerated conversion noted as the system's memory effect increases and the derivative order is under 1. This analysis highlights that fractional-order dynamics combined with memory effects outperform integer-order dynamics across varying values and initial species concentrations.

The model compartment comparison simulations for different fractional orders for the CPC and Caputo operator are displayed in Fig. 14,15,16,...,25. These simulation results are also displayed in Tables 1,2,3,...,12. These visualizations show that the CPC operator outperforms the Caputo operator. The extra degree of freedom that fractional-order parameters offer gives fractional order a benefit by adding more in-depth information to the study in new dimensions. The research facilitates the analysis of complex real-world problems and the effective prediction of associated tactics.

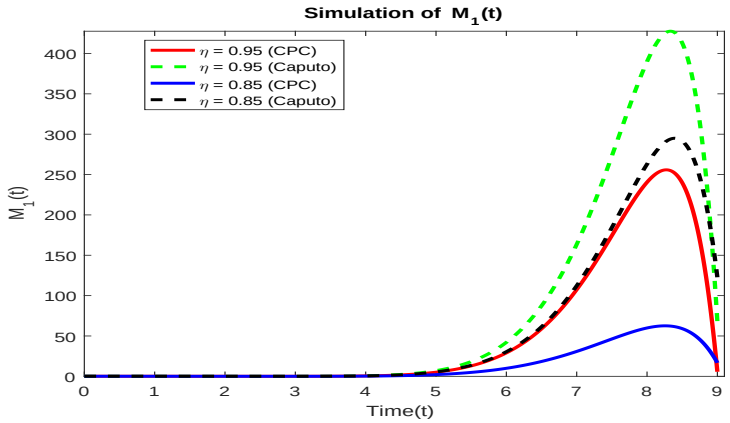

Fig. 14: Simulation of MnO_4^- using fructose data at CPC and Caputo operator

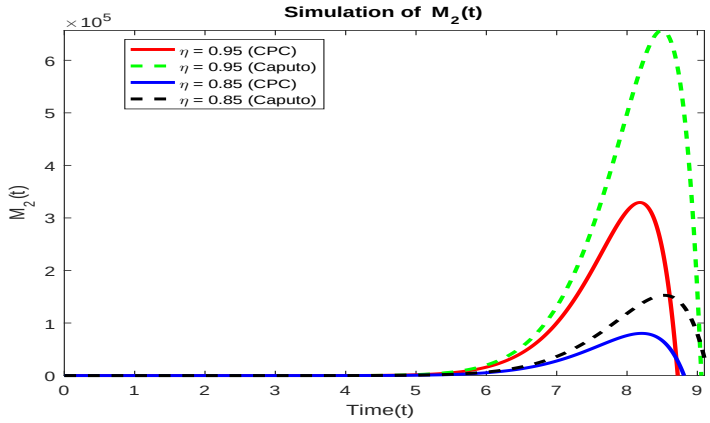

Fig. 15: Simulation of MnO_4^{2-} using fructose data at CPC and Caputo operator

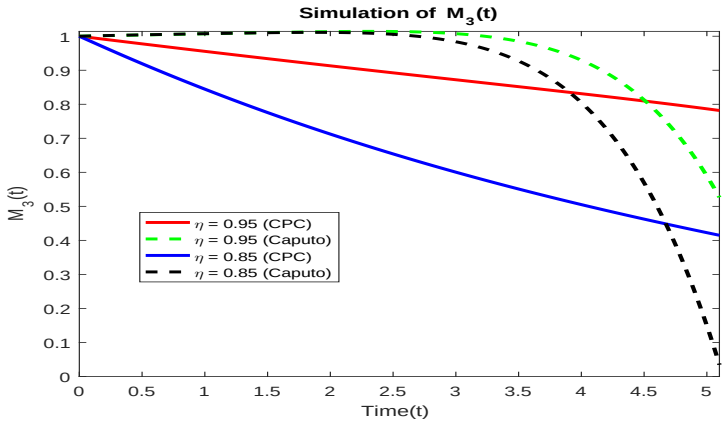

Fig. 16: Simulation of $Mn_{(aq)}^{(IV)}$ using fructose data at CPC and Caputo operator

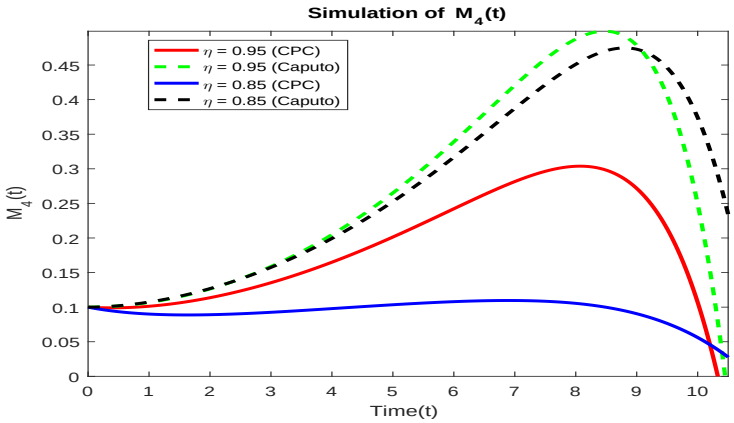

Fig. 17: Simulation of MnO_2 using fructose data at CPC and Caputo operator

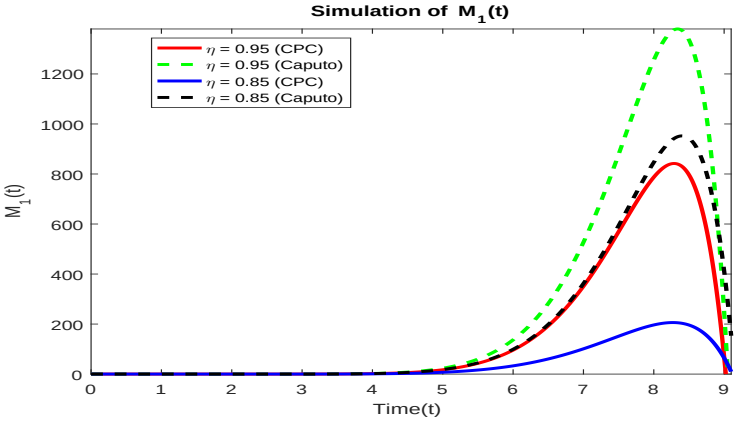

Fig. 18: Simulation of MnO_4^- using glucose data at CPC and Caputo operator

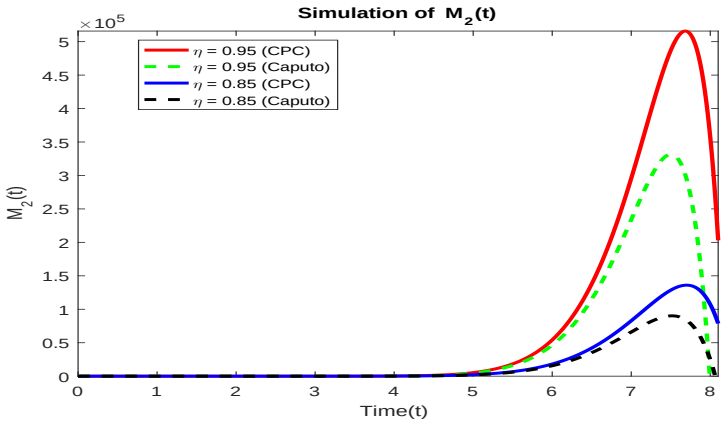

Fig. 19: Simulation of MnO_4^{2-} using glucose data at CPC and Caputo operator

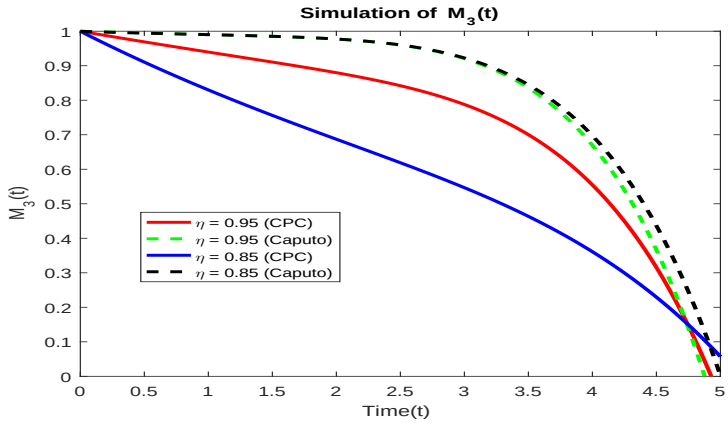

Fig. 20: Simulation of $Mn_{(aq)}^{(IV)}$ using glucose data at CPC and Caputo operator

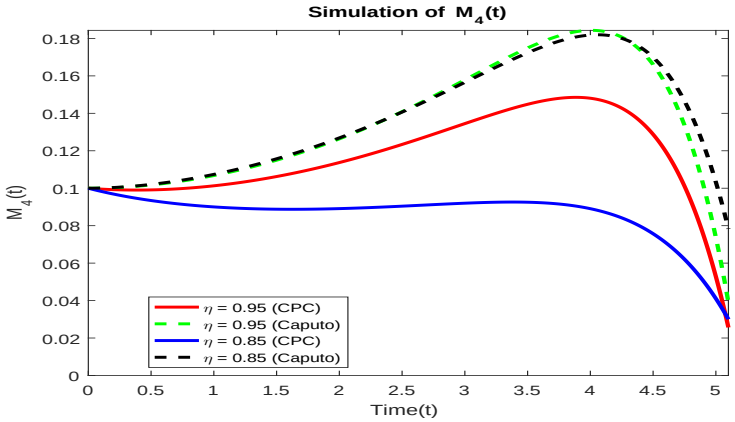

Fig. 21: Simulation of MnO_2 using glucose data at CPC and Caputo operator

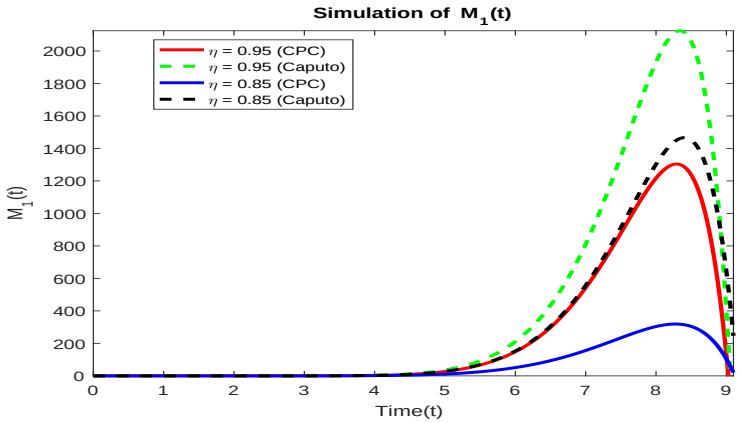

Fig. 22: Simulation of MnO_4^- using sucrose data at CPC and Caputo operator

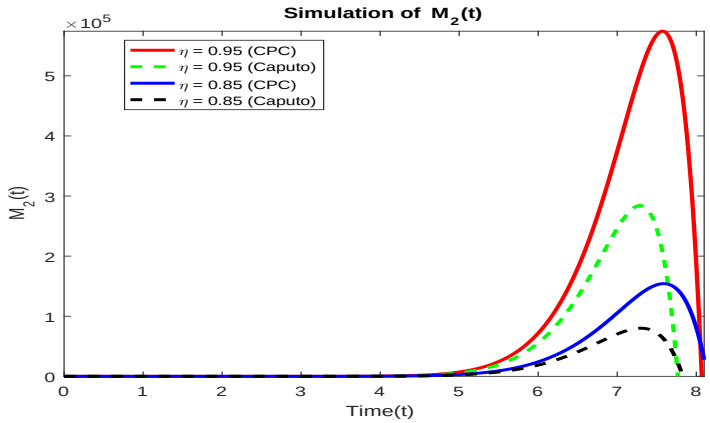

Fig. 23: Simulation of MnO_4^{2-} using sucrose data at CPC and Caputo operator

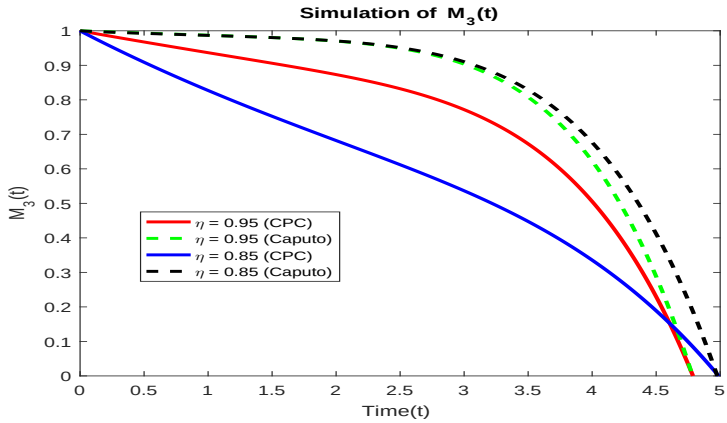

Fig. 24: Simulation of $Mn_{(aq)}^{(IV)}$ using sucrose data at CPC and Caputo operator

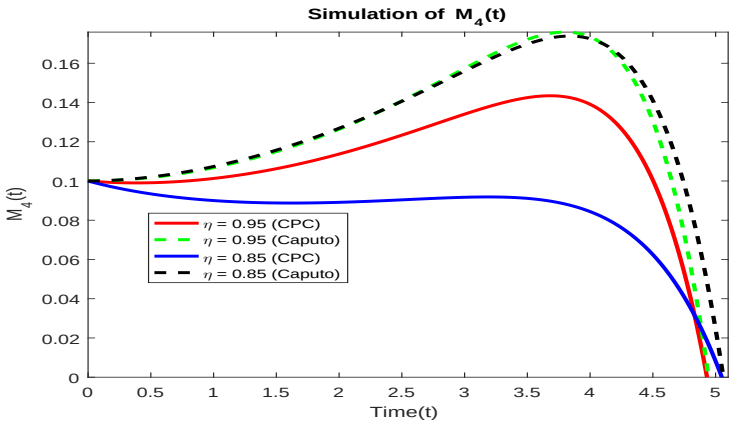

Fig. 25: Simulation of MnO_2 using sucrose data at CPC and Caputo operator

Table 1: Comparison of numerical simulations of MnO_4^- with fructose data

Time (t)	$\eta = 0.95$		$\eta = 0.85$	
	CPC	Caputo	CPC	Caputo
0.0	0.1000	0.1000	0.1000	0.1000
2.0	0.0494	0.0687	0.0497	0.0674
4.0	0.5308	0.6602	0.2716	0.5634
6.0	29.009	42.116	9.9482	30.461
8.0	240.52	390.05	59.912	262.82
9.0	5.6592	67.668	16.723	123.40

Table 2: Comparison of numerical simulations of MnO_4^{2-} with fructose data

Time (t)	$\eta = 0.95$		$\eta = 0.85$	
	CPC	Caputo	CPC	Caputo
0.0	0.2000	0.2000	0.2000	0.2000
2.0	0.2229	0.2484	0.1763	0.2498
4.0	77.800	94.543	40.821	49.900
6.0	1.602e+04	1.996e+04	5371.1	6693.2
8.0	3.131e+05	4.984e+05	7.615e+04	1.181e+05
8.5	2.415e+05	3.715e+05	6.665e+04	1.114e+05

Table 3: Comparison of numerical simulations of $Mn_{(aq)}^{(IV)}$ with fructose data

Time (t)	$\eta = 0.95$		$\eta = 0.85$	
	CPC	Caputo	CPC	Caputo
0.0	1.0000	1.0000	1.0000	1.0000
1.0	0.9556	1.0071	0.8445	1.0073
2.0	0.9131	1.0143	0.7124	1.0011
3.0	0.8721	1.0080	0.6005	0.9837
4.0	0.8311	0.9295	0.5051	0.8053
5.0	0.7867	0.5894	0.4227	0.1491

Table 4: Comparison of numerical simulations of MnO_2 with fructose data

Time (t)	$\eta = 0.95$		$\eta = 0.85$	
	CPC	Caputo	CPC	Caputo
0.0	0.1000	0.1000	0.1000	0.1000
2.0	0.1137	0.1263	0.0891	0.1268
4.0	0.1652	0.2048	0.0979	0.1993
6.0	0.2422	0.3390	0.1079	0.3167
8.0	0.3036	0.4875	0.1055	0.4512
10	0.1069	0.2490	0.0561	0.3741

Table 5: Comparison of numerical simulations of MnO_4^- with glucose data

Time (t)	$\eta = 0.95$		$\eta = 0.85$	
	CPC	Caputo	CPC	Caputo
0.0	0.1000	0.1000	0.1000	0.1000
2.0	0.0638	0.0628	0.0485	0.0602
4.0	1.8580	2.3055	0.9543	1.9642
6.0	95.952	136.88	32.911	99.122
8.0	787.01	1255.1	196.40	846.50
9.0	69.112	250.30	64.512	412.21

Table 6: Comparison of numerical simulations of MnO_4^{2-} with glucose data

Time (t)	$\eta = 0.95$		$\eta = 0.85$	
	CPC	Caputo	CPC	Caputo
0.0	0.2000	0.2000	0.2000	0.2000
2.0	0.2628	0.2869	0.2112	0.2895
4.0	279.10	246.52	146.40	129.80
6.0	5.419e+04	4.637e+04	1.819e+04	1.559e+04
8.0	3.569e+05	1.395e+05	1.072e+05	2.457e+04

Table 7: Comparison of numerical simulations of $Mn_{(aq)}^{(IV)}$ with glucose data

Time (t)	$\eta = 0.95$		$\eta = 0.85$	
	CPC	Caputo	CPC	Caputo
0.0	1.0000	1.0000	1.0000	1.0000
1.0	0.9396	0.9903	0.8298	0.9900
2.0	0.8798	0.9973	0.6869	0.9773
3.0	0.7877	0.9202	0.5466	0.9225
4.0	0.5547	0.6695	0.3611	0.6972
5.0	0.0656	0.0866	0.0574	0.0019

Table 8: Comparison of numerical simulations of MnO_2 with glucose data

Time (t)	$\eta = 0.95$		$\eta = 0.85$	
	CPC	Caputo	CPC	Caputo
0.0	0.1000	0.1000	0.1000	0.1000
1.0	0.1013	0.1068	0.0902	0.1075
2.0	0.1138	0.1265	0.0893	0.1279
3.0	0.1345	0.1579	0.0921	0.1566
4.0	0.1481	0.1843	0.0891	0.1818
5.0	0.0528	0.0737	0.4106	0.1033

Table 9: Comparison of numerical simulations of MnO_4^- with sucrose data

Time (t)	$\eta = 0.95$		$\eta = 0.85$	
	CPC	Caputo	CPC	Caputo
0.0	0.1000	0.1000	0.1000	0.1000
2.0	0.0646	0.0606	0.0489	0.0583
4.0	2.9380	3.6431	1.5111	3.1042
6.0	148.70	211.16	51.032	153.20
8.0	1217.1	1932.5	303.93	1302.9
9.0	129.60	399.80	104.12	642.52

Table 10: Comparison of numerical simulations of MnO_4^{2-} with sucrose data

Time (t)	$\eta = 0.95$		$\eta = 0.85$	
	CPC	Caputo	CPC	Caputo
0.0	0.2000	0.2000	0.2000	0.2000
2.0	0.2777	0.2998	0.2246	0.3027
4.0	376.53	308.51	197.70	162.50
6.0	7.182e+04	5.558e+04	2.412e+04	1.87e+04
7.0	3.747e+05	2.463e+05	1.053e+05	7.029e+04
8.0	1.875e+05	9.239e+04	8.104e+04	1.124e+04

Table 11: Comparison of numerical simulations of $Mn_{(aq)}^{(IV)}$ with sucrose data

Time (t)	$\eta = 0.95$		$\eta = 0.85$	
	CPC	Caputo	CPC	Caputo
0.0	1.0000	1.0000	1.0000	1.0000
1.0	0.9366	0.9872	0.8271	0.9867
2.0	0.8732	0.9701	0.6820	0.9706
3.0	0.7716	0.9034	0.5364	0.9104
4.0	0.5055	0.6227	0.3355	0.6767
4.5	0.2296	0.2861	0.1889	0.4119

Table 12: Comparison of numerical simulations of MnO_2 with sucrose data

Time (t)	$\eta = 0.95$		$\eta = 0.85$	
	CPC	Caputo	CPC	Caputo
0.0	0.1000	0.1000	0.1000	0.1000
1.0	0.1013	0.1068	0.0901	0.1074
2.0	0.1137	0.1264	0.0891	0.1269
3.0	0.1341	0.1573	0.0917	0.1560
4.0	0.1391	0.1734	0.0844	0.1725
4.5	0.1004	0.1306	0.0625	0.1411

6 Conclusion

This study expanded the permanganate oxidation reaction model and analyzed its solution using the LADM approach. The study used CPC fractional operator to analyze the solution. Qualitative features such as existence, uniqueness, and generalized Ulam-Hyers-Rassias stability were found in solutions. The hybrid fractional operators' simulation results for various fractional values were compared, and numerical results were presented in tables. LADM is an excellent

analytical method for dealing with nonlinear systems of fractional order. The determined solution of the fractional order model provides a strong computational mechanism for understanding physical problems and is manageable, simple to use, and accurate. Hybrid fractional operators produce outstanding results in mathematical modelling of oxidation kinetics, potentially better capturing phenomena than the integer-order model due to its greater memory. Compared to classical models, fractional models provide a wide range of solutions, enabling an improved fit between conceptual and actual data. By altering fractional parameters, one can improve interpretations for oxidation processes using the CPC fractional differential operator. Chemical reactions that take place on a commercial scale can be studied in future studies. Reactions in big reactors can be modeled using the approach under examination. Current models can be solved with more generalized operators. This study could be expanded to include fractional operators that are more broadly applicable and improve the control techniques for sugar oxidation. Without offering any real-world examples of parameter fitting, the study is theoretical and concentrates on the mathematical structure of fractional-order models. The methodology for calculating the parameters of the CPC fractional derivative and fractional order σ can be applied to time-resolved experimental data using well-established numerical optimization techniques in the future.

References

[1] S. Dash, S. Patel, and B. K. Mishra, Oxidation by permanganate: synthetic and mechanistic aspects. *Tetrahedron*, **65**(4), 707-739, (2009).
[2] K. C. Huang, G. E. Hoag, P. Chheda, B. A. Woody, and G. M. Dobbs, Kinetics and mechanism of oxidation of tetrachloroethylene with permanganate. *Chemosphere*, **46**(6), 815-825, (2002).
[3] S. Gharby, A. Asbbane, M. N. Ahmed, J. Gagour, O. Hallouch, S. Oubannin, and M. Ibourki, Vegetable oil oxidation: Mechanisms, impacts on quality, and approaches to enhance shelf life. *Food Chemistry: X*, 102541, (2025).
[4] R. Varala, S. Dhadda, V. Seema, M. Amanullah, M. Hussien, and N. M. Alam, Recent advances in metal-mediated oxidations with m CPBA. *Transition Metal Chemistry*, **49**(6), 395-428, (2024).
[5] J. F. Yang, M. He, T. F. Wu, A. P. Hao, S. B. Zhang, Y. D. Chen, and L. Deng, Sulfadiazine oxidation by permanganate: kinetics, mechanistic investigation and toxicity evaluation. *Chemical Engineering Journal*, **349**, 56-65, (2018).
[6] X. Guan, D. He, J. Ma, G. Chen, Application of permanganate in the oxidation of micropollutants: a mini review. *Frontiers of Environmental Science & Engineering in China*, **4**(4), 405-413, (2010).
[7] Y. Wang, K. Zheng, H. Guo, L. Tian, Y. He, X. Wang, Y. Liu, Potassium permanganate-based advanced oxidation processes for wastewater decontamination and sludge treatment: a review. *Chemical Engineering Journal*, **452**, 139529, (2023).
[8] J. Li, S. Y. Pang, Z. Wang, Q. Guo, J. Duan, S. Sun, and J. Jiang, Oxidative transformation of emerging organic contaminants by aqueous permanganate: Kinetics, products, toxicity changes, and effects of manganese products. *Water Research*, **203**, 117513, (2021).
[9] H. K. Okoro and E. O. Odebunmi, Kinetics and mechanism of oxidation of sugar and sugar alcohols by $KMnO_4$. *Int. J. Phys. Sci.*, **4**(9), 474-476, (2009).
[10] M. S. Manhas and Mohammed, F. A kinetic study of oxidation of β-cyclodextrin by permanganate in aqueous media. *Colloids and Surfaces A: Physicochemical and Engineering Aspects*, **295**(1-3), 165-171, (2007).
[11] R. R. Shaban, M. M. Abdelwahab, and S. M. Ibrahim, Synthesis of Oxalic from Sugarcane Molasses by Oxidation-reduction Reactions using Permanganate Ion as Oxidant. *Egyptian Sugar Journal*, **16**, 27-40, (2021).
[12] A. Rafia, N. Raheela, Q. Noshab, and M. Imran, Kinetics and mechanisms of oxidation of d-fructose and d-lactose by permanganate ion in acidic medium. *Natural Science*, **2012**, (2012).
[13] G. Yao, K. M. Bliss, M. Crimi, K. R. Fowler, J. Clark-Stone, W. Li, and P. J. Evans, Radial basis function simulation of slow-release permanganate for groundwater remediation via oxidation. *Journal of Computational and Applied Mathematics*, **307**, 235-247, (2016).
[14] N. Gheibi, N. Emrani, M. Eftekhari, M. Akrami, J. Abdollahi, M. Ramezani, and A. Sedghian, Experimental investigation and mathematical modeling for microbial removal using potassium permanganate as an oxidant case study: water treatment plant No. 1, Mashhad, Iran. *Environmental monitoring and assessment*, **191**(3), 141, (2019).
[15] S. T. McBeath, D. P. Wilkinson, and N. J. Graham, Advanced electrochemical oxidation for the simultaneous removal of manganese and generation of permanganate oxidant. *Environmental Science: Water Research & Technology*, **6**(9), 2405-2415, (2020).
[16] J. Milek, Estimation of the kinetic parameters for H_2O_2 enzymatic decomposition and for catalase deactivation. *Brazilian Journal of Chemical Engineering*, **35**(3), 995-1004, (2018).
[17] N. D. Pham, M. I. H. Khan, and M. A. Karim, A mathematical model for predicting the transport process and quality changes during intermittent microwave convective drying. *Food chemistry*, **325**, 126932, (2020).
[18] J. A. Miller, R. Sivaramakrishnan, Y. Tao, C. F. Goldsmith, M. P. Burke, A. W. Jasper, and J. Zádor, Combustion chemistry in the twenty-first century: Developing theory-informed chemical kinetics models. *Progress in Energy and Combustion Science*, **83**, 100886, (2021).
[19] C. Maharajan, C. Sowmiya, and C. Xu, Delay dependent complex-valued bidirectional associative memory neural networks with stochastic and impulsive effects: An exponential stability approach. *Kybernetika*, **60**(3), 317-356, (2024).

[20] C. Maharajan, C. Sowmiya, and C. Xu, Lagrange stability of inertial type neural networks: A Lyapunov-Krasovskii functional approach. *Evolving Systems*, **16**(2), 63, (2025).
[21] K. S. Nisar, M. Farman, K. Jamil, S. Jamil, and E. Hinçal, Fractional-order PID feedback synthesis controller including some external influences on insulin and glucose monitoring. *Alexandria Engineering Journal*, **113**, 60-73, (2025).
[22] M. Farman, C. Xu, P. Abbas, A. Sambas, F. Sultan, and K. S. Nisar, Stability and chemical modeling of quantifying disparities in atmospheric analysis with sustainable fractal fractional approach. *Communications in Nonlinear Science and Numerical Simulation*, **142**, 108525, (2025).
[23] J. X. Zhang, X. Zhang, D. Boutat, and D. Y. Liu, Fractional-order complex systems: Advanced control, intelligent estimation and reinforcement learning image-processing algorithms. *Fractal and Fractional*, **9**(2), 67, (2025).
[24] A. Hasan, M. Azeem, S. U. Saqib, M. M. Akram, An analysis of the Caputo Fabrizio fractional modeling for infectious diseases caused by chlamydia. *Journal of Mathematical Modeling and Fractional Calculus*, **1**(2), 99-118, (2024).
[25] M. Farman, K. S. Nisar, M. Ali, H. Ahmad, M. F. Tabassum, and A. S. Ghaffari, Chaos and forecasting financial risk dynamics with different stochastic economic factors by using fractional operator. *Modeling Earth Systems and Environment*, **11**(2), 146, (2025).
[26] D. Maya-Franco, E. Martínez-Guerrero, G. H. Sun, and S. H. Dong, Exploring Quantum Information Entropy in Double Hyperbolic Potentials Under the Fractional Schr"odinger Framework. *International Journal of Quantum Chemistry*, **125**(15), e70086, (2025).
[27] R. Santana-Carrillo, D. Maya-Franco, G. H. Sun, and S. H. Dong, Shannon and Fisher Entropy for a New Class of Single Hyperbolic Potentials in Fractional Schr"odinger Equation. *International Journal of Quantum Chemistry*, **125**(7), e70024, (2025).
[28] R. Santana-Carrillo, J. V. Peto, G. H. Sun, and S. H. Dong, Quantum information entropy for a hyperbolic double well potential in the fractional Schr"odinger equation. *Entropy*, **25**(7), 988, (2023).
[29] F. Al-Basir, A. M. Elaiw, D. Kesh, and P. K. Roy, Optimal control of a fractional-order enzyme kinetic model. *Control and Cybernetics*, 44(4), (2015).
[30] A. Akgül and S. A. Khoshnaw, Application of fractional derivative on non-linear biochemical reaction models. *International Journal of Intelligent Networks*, **1**, 52-58, (2020).
[31] J. Singh, M. M. Rashidi, D. Kumar, and R. Swroop, A fractional model of a dynamical Brusselator reaction-diffusion system arising in triple collision and enzymatic reactions. *Nonlinear Engineering*, **5**(4), 277-285, (2016).
[32] F. Rabah, M. Abukhaled, and S. A. Khuri, Solution of a complex nonlinear fractional biochemical reaction model. *Mathematical and Computational Applications*, **27**(3), 45, (2022).
[33] D. Baleanu, A. Fernandez, and A. Akgül, On a fractional operator combining proportional and classical differintegrals. *Mathematics*, **8**(3), 360, (2020).
[34] P. A. Naik, A. Zehra, M. Farman, A. Shehzad, S. Shahzeen, and Z. Huang, Forecasting and dynamical modeling of reversible enzymatic reactions with a hybrid proportional fractional derivative. *Frontiers in Physics*, **11**, 1307307, (2024).
[35] C. Xu, M. Liao, M. Farman, and A. Shehzade, Hydrogenolysis of glycerol by heterogeneous catalysis: a fractional order kinetic model with analysis. *MATCH Commun. Math. Comput. Chem*, **91**(3), 635-664, (2024).
[36] D. Kumar, H. Nama, and D. Baleanu, A reliable computational approach for fractional isothermal chemical model. *Alexandria Engineering Journal*, **108**, 364-370, (2024).
[37] R. J. Fernández-Terán, E. Sucre-Rosales, L. Echevarria, F. E. and Hernández, A sweet introduction to the mathematical analysis of time-resolved spectra and complex kinetic mechanisms: The chameleon reaction revisited. *Journal of Chemical Education*, **99**(6), 2327-2337, (2022).
[38] C. Li, D. Qian, and Y. Chen, On Riemann-Liouville and caputo derivatives. *Discrete Dynamics in Nature and Society*, **2011**(1), 562494, (2011).
[39] M. Arif, P. Kumam, and W. Watthayu, Analysis of constant proportional Caputo operator on the unsteady Oldroyd-B fluid flow with Newtonian heating and non-uniform temperature. *ZAMM-Journal of Applied Mathematics and Mechanics/Zeitschrift für Angewandte Mathematik und Mechanik*, **104**(2), e202300048, (2024).
[40] I. Siddique A. and Akgül, Analysis of blood liquor model via nonlocal and singular constant proportional Caputo hybrid differential operator. *Mathematical Methods in the Applied Sciences*, **46**(7), 7741-7750, (2023).
[41] S. Abdal, M. F. Tabassum, and A. Shahzad, Hybrid Fractional Operator for Epidemic Model analysis and application. *Journal of Mathematical Modeling and Fractional Calculus*, **1**(1), 25-37, (2024).
[42] R. Prabha and S. Kiruthika, Expression of Constant Proportional Caputo Derivative in Terms of the Block Pulse Operational Matrix. *IAENG International Journal of Applied Mathematics*, **55**(8), 2635-2644, (2025).
[43] Y. Zhao, C. Xu, Y. Xu, J. Lin, Y. Pang, Z. Liu, and J. Shen, Mathematical exploration on control of bifurcation for a 3D predator-prey model with delay. *AIMS Math*, **9**(11), 29883-29915, (2024).
[44] J. Lin, C. Xu, Y. Zhao, and Q. Deng, Hopf bifurcation and controller design for a predator prey model with double delays, *AIP Advances*, **15**(7), (2025).